European Conference on Optical Communication (ECOC) 2022 © Optica Publishing Group 2022

Spectro-temporally Multiplexed Reservoir Computing Based on a Multimode Fabry Perot Laser

M. Skontranis(1), G. Sarantoglou(1), A. Bogris(2), C. Mesaritakis(1)

(1) University of the Aegean, Dept. of Information and Communication Systems Engineering, Palama 2, Samos-83200 Greece, mskontranis@icsd.aegean.gr
(2) University of West Attica, Dept. Informatics and Computer Engineering, Ag. Spiridonos, Egaleo, 12243-Greece.

Abstract *We present numerical results from a spectro-temporal reservoir computing based on a Fabry-Perot laser. By exploiting longitudinal modes, we achieved tunable real time processing rate, reaching up to 2.38 GHz for an image classification task with elevated accuracy.*

Introduction

In the last two decades, Artificial Neural Networks (ANNs) have drawn the spotlight of attention of many research groups since they can efficiently address nonlinear and highly demanding problems. In particular, they have achieved high or even superhuman performance at tasks such as voice recognition, image classification and channel equalization. Their unprecedented performance is attributed to the parallel work of multiple interconnected nonlinear nodes. However, the large number of neurons along with millions of tunable synaptic weights rise a question with regards to ANN's efficient handling. Classical Von Neuman processors face difficulties upon this task due to their sequential processing which violates the parallel function of the ANN. Moreover, tracking of multiple parameters and outputs results in complex hardware layouts with power hungry demands especially during the training phase [1].

In the last years, a specific discipline of the ANN field, known as Reservoir Computing (RC), has been the research subject of multiple scientific groups. In classical RC networks, neurons are divided in three layers: the input layer, where the insertion of the input data takes place, the RC layer, which consists of multiple sparsely connected neurons with fixed random synaptic weights and the output layer which determines the state of the network. In RC networks, only the neurons of the output layer are trained, resulting to less time and power consuming training, whereas random synapses render them hardware friendly [2]. Based on these advantages, photonic platforms were among the first adopters of the RC paradigm; combining their ultra-high bandwidth, low power consumption and integration capabilities with RC's robustness and efficiency [2].

Photonic RC implementations are divided in two major categories: the first one is the spatial RC, in which every node is represented by a physical component [2]. This type of RCs has demonstrated enhanced performance in time series analysis (pattern recognition and chaotic series prediction etc). Nonetheless, upscaling remains a challenge. The second category is Time-Delay RC (TDRC) in which the entire hidden layer is replaced by a single nonlinear node equipped with a feedback loop. In this case, nodes are time multiplexed resulting to minimum hardware requirements. The number of these virtual nodes is regulated by the length of the feedback loop alongside the unavoidable speed penalty due to time stretching [2]. Previous TDRC implementations were based on VCSELs [3], spin VCSELs [4], microring [5] and phased array lasers [6]. Recently, our group has published a TDRC scheme based on a multimode Fabry-Perot (FP) laser, where speed penalty was minimized by exploiting the multiple longitudinal modes [7].

In this paper, we extend the aforementioned multimode concept to image processing, by assigning each longitudinal mode to a different pixel, thus unlocking spatial information processing by a spectro-temporal multiplexing. Numerical simulations targeting the MNIST dataset, validated that an integration ready TDRC based on this approach can offer tunable processing rate, ranging from 2.38 Gframes / s (Gfr/s) with 92.87% accuracy to 85 Mfr/s with 95.33% accuracy. These results are superior to stand alone Fully Connected Layer (FCL) thus confirming photonic acceleration with a simultaneous improvement by means of nonlinear processing. At the same time processing rate surpasses the state-of-the-art TDRCs [6,8].

FP TDRC Numerical Model

The simulation of the FP laser is based on [7]. More specifically, for a M-mode FP laser a total of $M+1$ rate equations are needed to monitor its outputs. M equations describe the time evolution

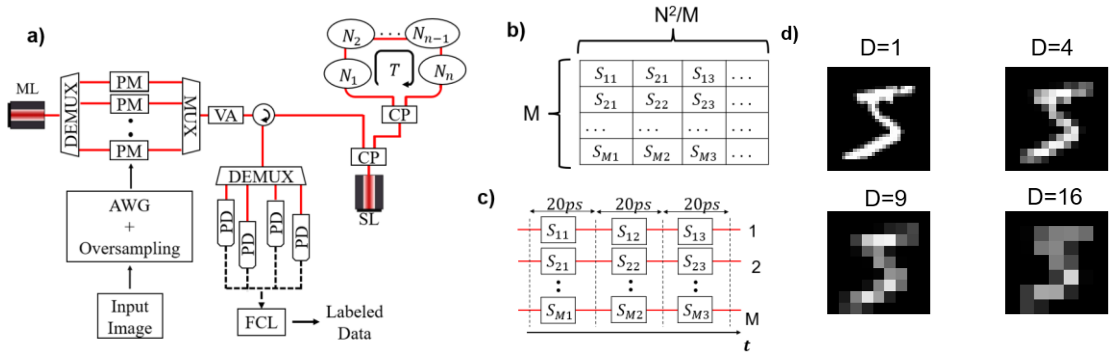

Fig. 1: a) The layout of the spectrotemporally multiplexed TDRC. Phase Modulators (PM), Variable Attenuator (VA), Coupler 2x 1 (CP), Arbitrary Waveform Generator (AWG) and Photodiode (PD). b) Redistributed input of the TDRC c) Distribution of pixels intensity S_{XY} among the modes of the FP. d) Downsampled images D=1 stands for the original input image.

of the corresponding M electrical fields while the last equation stands for the time evolution of the carriers. Our model is summarized in the following equations:

$$\dot{E_m} = \frac{1+ia}{2}\left[G_m(t) - \frac{1}{t_{ph}}\right]E_m(t) + \frac{k_f}{t_{rt}}E_m(t-T)e^{i\omega_m T}$$

$$+\frac{k_{inj}}{t_{rt}}E_{inj}(t)e^{-i\Delta\omega_m t} + \sqrt{2\beta N(t)}\xi(t) \quad : (1)$$

$$\dot{N(t)} = \frac{I}{q} - \frac{N(t)}{t_n} - \sum_{1-M/2}^{M/2} G_m(t)|E_m(t)|^2 : (2)$$

$$G_m(t) = \frac{g[N(t)-N_0]}{1+s\sum_{1-M/2}^{M/2}|E_m(t)|^2}\left[1-\left(\frac{\Delta f_L}{\Delta f_g}\right)^2\right] \quad : (3)$$

where m is the index of the longitudinal mode whereas E_m, ω_m and G_m are the envelope of the complex electrical field, oscillation frequency and gain of the m^{th} longitudinal mode respectively. N is the total number of carriers inside the cavity. The used values for all the parameters are given in [7]. In our model coherent mixing phenomena are neglected due to the high value of the Free Spectral Range which is set to 128 GHz [9].

The overall architecture of the proposed TDRC is presented in Fig.1a. It consists of two FP lasers in a Master-Slave (ML-SL) configuration. The M outputs of the ML, which correspond to the M longitudinal modes of the FP are phase modulated by the incoming data. Thus, each pixel's intensity is imprinted in different modes' phase (Fig.1a-1c), allowing parallel data insertion and processing. This is a key difference to all previous implementations where image data was inserted and processed in a sequential manner [2]. Following the TDRC paradigm, our method allows the reduction of processing latency by a factor R, which is equal to the number of the used longitudinal modes.

The outputs of the ML are injected to the SL whose output is divided in two directions by two 2x1 Couplers (CP) (Fig. 1a): the weaker output of the SL is used as feedback through the external loop whereas the stronger output is directed to a set of M photodiodes (PD). Each PD monitors the optical power of a specific longitudinal mode, after optical demultiplexing. PD bandwidth is set to 50GHz whereas thermal and shot noise have been also considered. In the simulations, the same injection and feedback strength is used, $k_{inj} = 0.75$ and $k_f = 0.01$ respectively while the length of the feedback was set to 120 ps for all cases.

Finally, the retrieved outputs are fed to a Fully Connected Layer (FCL) which determines the label of the input images. The data insertion rate is 50 GHz and the same sampling rate is used at the photodiodes. Therefore, the spacing of the virtual nodes is $\theta = 20\,ps$.

Preprocessing of the MNIST data

In this work, a preprocessing was applied to the original data so as to further reduce the number of inputs and processing latency of the proposed TDRC. In particular, we divided the original MNIST image in several square sections whose area consisted of $S = 4{,}9$ and 16 pixels. For each square section we calculated the mean intensity of the corresponding pixels and that value was used as input to the TDRC. Consequently, for $S = 4, 9, 16$ the original MNIST image was compressed by a factor $D = S$ (Fig. 1d), leading to a 196-, 81- and 49-pixel image respectively. After that, a redistribution of the input image was performed transforming the NxN input image to a MxN' (Fig. 1c) where N' is the rounding of the quotient N^2/M towards the higher integer. The m^{th} line of the MxN' input image determines the pixels that are going to be processed by the m^{th} mode. Finally, an oversampling of the input image by 3 was applied followed by the necessary masking procedure, which is typical in all TDRC schemes (Fig.1a). The oversampling of the input image was performed per column. In Table 1 we present the

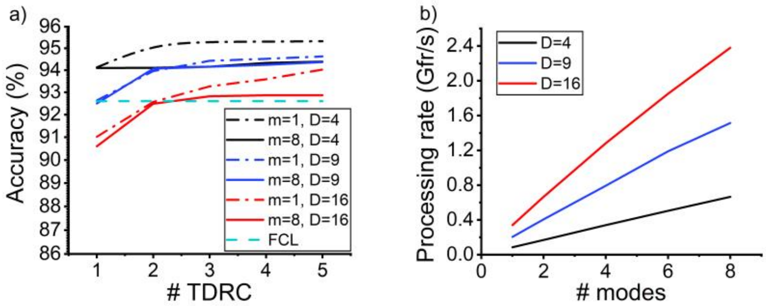

Figure 2: (a) Classification accuracy for one (solid) and eight (solid and dot) longitudinal modes for multiple TWM TDRCs. The cyan dotted line designates the baseline of the evaluation process. (b) Processing rate per image for different number of longitudinal modes.

number of input pixels for different compression factors D along with the inputs of the FCL layer. The difference between the inputs to the FCL for different values of M is due to the rounding of the N^2/M. It is worth mentioning that in all cases the number of FCL inputs are lower compared to a typical standalone FCL treating MNIST data (784). Therefore, hardware simplification and processing acceleration can be achieved.

Tab. 1: Number of inputs to the TDRC before oversampling and inputs to the FCL.

D	Inputs to the TDRC	FCL inputs (I_{FCL}) (M=1,M=2,M=4,M=6,M=8)
4	196	588, 588, 588, 588,600
9	81	243, 246, 252, 252, 264
16	49	147, 150, 156, 162, 168

Results

In this section, numerical results regarding the performance of the proposed TDRC are presented. From the 70000 images of the MNIST database 49000 were used for training, 7000 for validation and 14000 for testing. We evaluated the performance of our network for three different compressing factors $(D = 4{,}9{,}16)$ and for two numbers of longitudinal modes $(M = 1, 8)$. The baseline of the evaluation was set to 92.6% which is the classification accuracy of the MNIST database for a standalone FCL targeting an uncompressed image (Fig. 2a cyan dashed line).

In Fig.2a the classification accuracy of our network is presented for different values of the D and M parameters versus the number of parallel TDRCs employed prior to the FCL. Specifically, the demonstrated results show that the performance degrades as D increases for both $M = 1$ and $M = 8$ which can be attributed to the degradation of the quality of the input image (Fig.1d). In particular, for a single mode FP $(M = 1)$ and for $D = 4{,}9$ and 16 our TDRC achieves 94.13%, 92.64% and 91.02% respectively whereas for an eight mode FP (M=8) we achieved 94.13%, 92.50% and 90.60%. Consequently, the single mode FP has a slight accuracy advantage over multimode FPs. To further meliorate their performance, we added multiple TDRCs which used different masks. For $M = 1$, the second TDRC increases accuracy to 95.2%, 93.96% and 92.57% for $D = 4{,}9$ and 16 respectively whereas for $M = 8$ the accuracy is merely augmented to 94.04% for $D = 4$ while for $D = 9$ and $D = 16$ the achieved performance is measures at 94.17% and 92.49%. Lastly, the use of extra TDRCs provokes a marginal increase in accuracy for all cases with an exception of $M = 1$ and $D = 16$ where the increase is substantial, reaching up to 94.03% for 5 TDRCs.

From the above analysis, it is clear that the best accuracy occurs for $M = 1$. However, for $M = 8$, there is a significant processing acceleration equal to M. To quantize the accuracy – acceleration relation, we calculated the processing frequency of the proposed network f_{pr} for $M = 1{,}2{,}4{,}6$ and 8. f_{pr} was calculated as $f_{pr} = M/(I_{FCL} \cdot \theta)$ where I_{FCL} is the number of outputs of a single TDRC (Table 1). From Fig.2b we can see that f_{pr} steadily increases as M increases ranging from 85Mfr / s ($M = 1$ and $D = 4$) up to 2.38 Gfr / s ($M = 8$ and $D = 16$), higher than other TDRC implementations [6,8]. The critical aspect in this work, is that in all cases, TDRC accuracy remains always higher than the baseline (92.6%) for all measured cases even when image is compressed (D). Therefore, the f_{pr} of our TDRC is tunable and can be set according to the accuracy demands of the addressed task. At the same time the number of outputs is much smaller than other state-of-the-art works [6,8].

Conclusions

We present a spectro-temporal multiplexed TDRC. Our scheme boosts the performance of a standalone FCL at an image classification task whereas, it also increases its processing rate.

Acknowledgements

This work has received funding from the Neoteric H2020 project under grant agreement No 871330

References

[1] Abu-Mostafa, Y. S., & Psaltis, D. (1987). Optical neural computers. Scientific American, 256(3), 88-95. (1987)

[2] Tanaka, G., Yamane, T., Héroux, J. B., Nakane, R., Kanazawa, N., Takeda, S., ... & Hirose, A. (2019). Recent advances in physical reservoir computing: A review. Neural Networks, 115, 100-123. DOI: doi.org/10.1016/j.neunet.2019.03.005

[3] Guo, X. X., Xiang, S. Y., Zhang, Y. H., Lin, L., Wen, A. J., & Hao, Y. (2019). Four-channels reservoir computing based on polarization dynamics in mutually coupled VCSELs system. Optics express, 27(16), 23293-23306. DOI: doi.org/10.1364/OE.27.023293

[4] Skontranis, M., Sarantoglou, G., Bogris, A., & Mesaritakis, C. (2022). Time-Delayed Reservoir Computing Based on Dual-Waveband Quantum-Dot Spin-Polarized Vertical Cavity Surface-Emitting Laser. *arXiv preprint arXiv:2203.16473*.

[5] Borghi, M., Biasi, S., & Pavesi, L. (2021). Reservoir computing based on a silicon microring and time multiplexing for binary and analog operations. Scientific Reports, 11(1), 1-12. DOI: doi.org/10.1038/s41598-021-94952-5

[6] Huang, Y., Zhou, P., Yang, Y., Chen, T., & Li, N. (2021). Time-Delayed Reservoir Computing Based on a Two-Element Phased Laser Array for Image Identification. IEEE Photonics Journal, 13(5), 1-9. DOI: doi.org/10.1038/s41598-021-94952-5

[7] Bogris, A., Mesaritakis, C., Deligiannidis, S., & Li, P. (2020). Fabry-Perot lasers as enablers for parallel reservoir computing. *IEEE Journal of Selected Topics in Quantum Electronics*, *27*(2), 1-7. DOI: 10.1109/JSTQE.2020.3011879

[8] Nakajima, M., Tanaka, K., & Hashimoto, T. (2021). Scalable reservoir computing on coherent linear photonic processor. Communications Physics, 4(1), 1-12. DOI : doi.org/10.1038/s42005-021-00519-1

[9] Li, P., Cai, Q., Zhang, J., Xu, B., Liu, Y., Bogris, A., Shore, A., Wang, Y. (2019). Observation of flat chaos generation using an optical feedback multi-mode laser with a band-pass filter. Optics Express, 27(13), 17859-17867. DOI: doi.org/10.1364/OE.27.017859